Lawrence Berkeley National Laboratory
Recent Work

Title

Interface Characterization of XUV Multilayer Reflectors Using HRTEM and X-ray and XUV Reflectance

Permalink

https://escholarship.org/uc/item/4d36q1mz

Authors

Windt, D.L.
Hull, R.
Waskiewicz, W.K.
et al.

Publication Date

1990-07-01
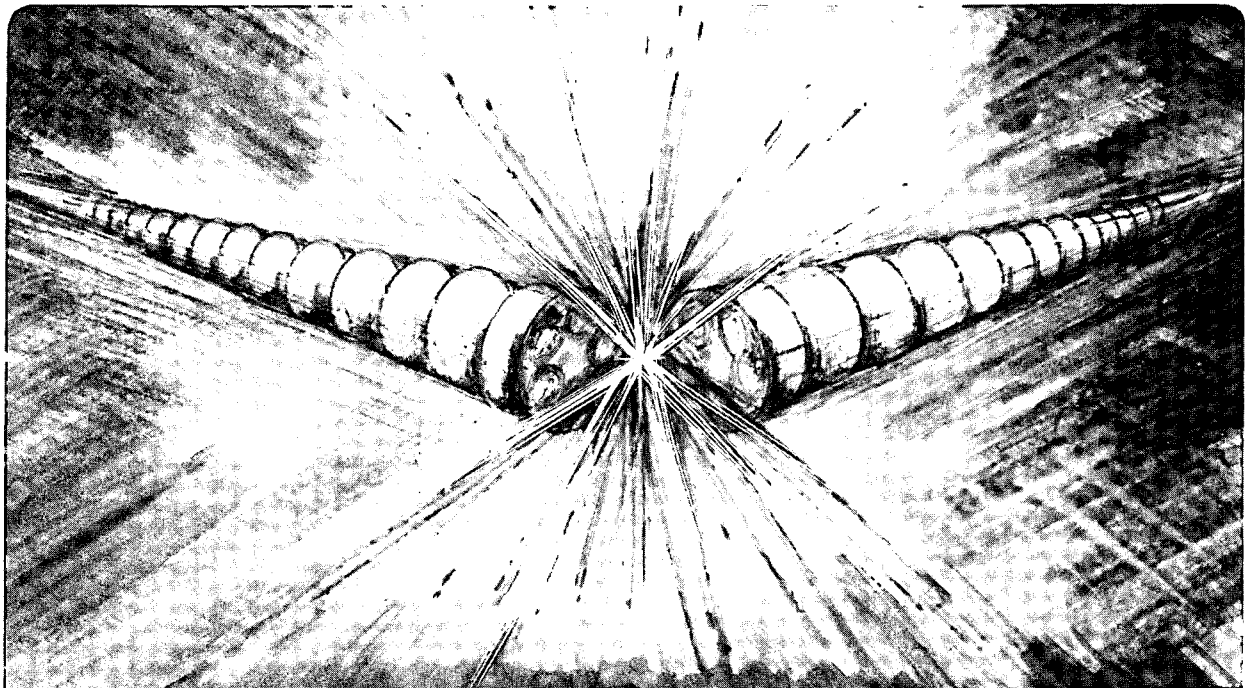
Lawrence Berkeley Laboratory
UNIVERSITY OF CALIFORNIA

Accelerator & Fusion Research Division

Interface Characterization of XUV Multilayer Reflectors Using HRTEM and X-ray and XUV Reflectance

D.L. Windt, R. Hull, W.K. Waskiewicz, and J.B. Kortright

July 1990

DISCLAIMER

This document was prepared as an account of work sponsored by the United States Government. While this document is believed to contain correct information, neither the United States Government nor any agency thereof, nor the Regents of the University of California, nor any of their employees, makes any warranty, express or implied, or assumes any legal responsibility for the accuracy, completeness, or usefulness of any information, apparatus, product, or process disclosed, or represents that its use would not infringe privately owned rights. Reference herein to any specific commercial product, process, or service by its trade name, trademark, manufacturer, or otherwise, does not necessarily constitute or imply its endorsement, recommendation, or favoring by the United States Government or any agency thereof, or the Regents of the University of California. The views and opinions of authors expressed herein do not necessarily state or reflect those of the United States Government or any agency thereof or the Regents of the University of California.

Interface characterization of XUV multilayer reflectors

using HRTEM and x-ray and XUV reflectance

D.L. Windt, R. Hull, and W.K. Waskiewicz
AT&T Bell Laboratories, Murray Hill, NJ 07974

and

J.B. Kortright
Lawrence Berkeley Laboratory, University of California, Berkeley, CA 94720

Interface characterization of XUV multilayer reflectors using HRTEM and x-ray and XUV reflectance

D. L. Windt, R. Hull and W. K. Waskiewicz
AT&T Bell Laboratories, Murray Hill, NJ 07974

and

J. B. Kortright
Lawrence Berkeley Laboratory, University of California, Berkeley, CA 94720

Abstract

We have examined the structure of XUV multilayer coatings using high-resolution transmission electron microscopy (HRTEM). Using a variety of techniques, we have measured the interface widths and the interface topography from the digitized TEM images, and have compared these results to x-ray and XUV reflectance measurements. We find that the structural parameters measured from the TEM images and those deduced from reflectance are consistent in light of the probable systematic errors associated with the measurement and interpretation techniques.

1 INTRODUCTION

Reflectance measurements of XUV multilayer coatings have revealed that the most significant limitation on the optical performance of these devices is that due to imperfect interfaces [1]. These interface imperfections — interfacial roughness and diffusion — reduce the XUV reflectance from the theoretical value by removing light from the specular direction. Reduced reflectance has obvious implications for multiple-reflection, multilayer-coated optical systems for soft x-ray projection lithography.

It is our objective to understand the structural details of interface imperfections in order to minimize their deleterious effect. In this paper we describe preliminary work involving quantitative analysis of high-resolution transmission electron micrographs of cross-sectional samples of XUV multilayer coatings. From the TEM images, we have measured the interface diffusion widths and the interface topography, and compared these structural parameters to the interface widths deduced from x-ray and XUV reflectance measurements.

In section II we outline the theoretical foundation on which our analysis is based. In particular, we describe how interface imperfections affect the distribution of scattered light, making use of a first-order vector scattering theory. In the sections following, we describe the experimental techniques used to obtain HRTEM images and reflectance data, the analysis of these data, and some preliminary results and conclusions.

2 THEORY

The scattering of light at an interface has been the subject of intensive research for many years [2]. A recent treatise by Stearns [3] on this subject makes use of a first-order Born approximation to solve the (vector) scattering problem for x-rays incident on an imperfect interface, and the results from that work are used here.

Interfacial roughness and diffusion remove light from the specular scattering direction. Interfacial roughness will also scatter light into non-specular directions. The result of Stearns' approach with regard to the specularly reflected light is that the reflection and transmission coefficients at the interface between two materials having different optical constants are given by

$$r = r_0 \cdot \tilde{w}(\Re\{-2kn_z^0\})$$
$$t = t_0 \tag{1}$$

where r_0 and t_0 are the usual Fresnel reflection and transmission coefficients, $k = 2\pi/\lambda$ (λ is the wavelength of light,) and $\tilde{w}$ is the Fourier transform of the derivative of the interface profile function $p(z)$, as described in [3]. (The incident field is assumed to be a plane wave propagating in the direction $\hat{n}^0$, so n_z^0 in equation 1 is that vector's component

along the $\hat{z}$-direction, which is normal to the plane of the interface.) For the special case where the interface profile is an error function,

$$p(z) = \frac{1}{\sqrt{\pi}} \int_{-\infty}^{z} e^{-t^2/2\sigma^2} dt,$$

where σ is the interface width, $\tilde{w}$ is given by

$$\tilde{w} = e^{-2(\frac{2\pi}{\lambda}\sigma \cos\theta)^2}$$

so that substitution into equation 1 yields the well-known result

$$r = r_0 \cdot e^{-2(\frac{2\pi}{\lambda}\sigma \cos\theta)^2} \tag{2}$$

Since $p(z)$ is defined as the normalized, *averaged* value of the dielectric function along the $\hat{z}$-direction, the modified Fresnel coefficients (equation 1) do not distinguish between a diffuse and a rough interface. Consequently, for the case of an interface which is both rough and diffuse, with an error-function interface profile for example, σ in equation 2 will be the sum of contributions from both interfacial roughness and diffusion:

$$\sigma_{\text{total}} = \sigma_{\text{rough}} + \sigma_{\text{diffuse}} \tag{3}$$

We can thus calculate the reflectance of a multilayer coating, using either the characteristic matrix or the recursive technique [4], making use of equation 1 to account for interface imperfections.

Another important result from Stearns describes the distribution of non-specular scattered light. We suppose that the interface topography is described by a function $f(x, y)$, with the power-spectral-density function, $S(f_x, f_y)$, given by

$$S(f_x, f_y) = \frac{\left|\tilde{f}(f_x, f_y)\right|^2}{L_x L_y} \tag{4}$$

where f_x and f_y are the spatial frequencies, and L_x and L_y are the linear dimensions of the interface, in the x and y directions, respectively. It is assumed that an incident plane wave propagates from medium ϵ_0 to ϵ_0' in a direction $\hat{n}^0$ with initial polarization $\hat{e}^0$, and scatters into a direction $\hat{n}$ with polarization $\hat{e}$. The differential power scattered per unit solid angle $d\Omega$ into the reflected ($n_z > 0$) field is then given by

$$\frac{1}{P_0}\frac{dP^r}{d\Omega} = \left\{ k^4 \cdot \left| \frac{(\epsilon_0 - \epsilon_0')(\hat{e}^* \cdot \hat{e}^0)}{16\pi^2 n_z^0 \epsilon_0} \right|^2 \right\} \cdot S(f_x, f_y) \tag{5}$$

with a similar expression for the transmitted ($n_z < 0$) scattered field. Equation 5 is the product of an 'optical factor', which depends on the wavelength, angles, and polarizations, and a 'surface factor', $S(f_x, f_y)$, which depends only on the interface topography. Similar results from other vector and scalar scattering theories have been obtained [2], all sharing this basic form of an optical factor times the power-spectral-density. Note that for the case of a multilayer, the non-specular scattered power distribution ($\frac{dP}{d\Omega}$) is determined by summing the contributions (equation 5) from each interface, taking into account the coherence of spatial frequencies between the layers.

3   EXPERIMENT

The experimental goal is to measure σ_{rough}, σ_{diffuse}, and $S(f_x, f_y)$, from quantitative analysis of HRTEM images of cross-sectional multilayer samples, and compare these, through equations 1 and 5, to the measured specular reflectance and non-specular scattered power distribution. We have thus far analyzed three multilayer samples. Described in this section are the experimental details of the sample fabrication and characterization.

Two Mo/Si and one Ru/C multilayer samples were fabricated by magnetron sputtering in argon, at AT&T Bell Labs, Lockheed, and the Center for X-Ray Optics at the Lawrence Berkeley Laboratory, respectively. The two Mo/Si samples contained 40 bilayers, with d-spacings of 74.5 Å and 93 Å. The Ru/C sample contained 50 bilayers and had a d-spacing of 44.25 Å. The Mo/Si samples were fabricated on semiconductor-grade Si (100) wafers, while the Ru/C sample was fabricated on a Si (111) wafer.

Small-angle x-ray reflectance measurements were made at AT&T Bell Labs using Cu-Kα (1.542 Å) radiation from a Rigaku rotating-anode source. A Huber four-circle diffractometer with a modified 1003-goniometer head positioned the sample and scintillation detector during the $\theta - 2\theta$ scans. Pyrolitic graphite was used as a monochromator, and precision slits provided a 0.05 mm horizontal x 0.5 mm vertical beam at the sample (scattering was done about a vertical axis), resulting in an angular resolution of about 0.025°. The detector signal was pulse-height-selected, and counting times were normalized against an I_0 detector to minimize source fluctuations. Measurements were made from 0-10° grazing, which corresponded to 8-15 Bragg peaks.

XUV reflectance measurements were made using the Lockheed reflectometer, which has been described previously [5]. Absolute reflectance versus incidence angle measurements from near-normal to grazing incidence were made at several wavelengths for each sample with this apparatus. Non-specular scattering measurements have not yet been performed, though measurements using synchrotron radiation at Brookhaven National Laboratory are being planned.

Cross-sectional multilayer samples, suitable for TEM analysis, were prepared by mechanical polishing followed by argon ion milling (4 keV at LN_2 temperature, incident beams at 15° to sample surface). Note that this technique results in varying sample thickness: the sample increases in thickness away from the hole left by the ion milling process. HRTEM was performed with JEOL 4000EX and 2000FX electron microscopes operated at 200 kV. The practical resolution limits of these microscopes at this energy are $\sim$2.0 Å and 3.0 Å, respectively.

Photographic prints of the HRTEM images were digitized using a CCD camera (512x480 pixels) and transferred to a Sun 4/260 workstation for analysis. The images were digitized such that the pixel size was at most equal to $\sim$half the resolution limit of the microscope. Due to non-uniform illumination during the image formation and digitization processes, it was necessary to subtract a two-dimensional polynomial (2nd-order) from the digitized images. Histogram equalization was then performed in order to increase the dynamic range of the images.

4 ANALYSIS

4.1 TEM Image Analysis

The objective here is to extract quantitative information relating to (i) the interface diffusion widths ($\sigma_{diffuse}$) and (ii) the interface topography (σ_{rough}, $S(f_x, f_y)$). To this end, we have developed two types of analyses of the digitized TEM images, and we describe each in turn. We first discuss, however, some limitations associated with HRTEM image interpretation.

4.1.1 TEM Image Interpretation

We would like to be able to relate the HRTEM image intensity at a given point to the projected crystal potential (which is in turn related to the material composition) of the sample at that point. However, there are a number of factors associated with the image formation that limit this type of intuitive image interpretation, and which give rise to systematic errors in the derived interface parameters.

An HRTEM image of a crystalline sample is formed by recombination of the phases and amplitudes of Bragg diffracted beams with the directly transmitted electron beam. In general, multiple scattering is very important in electron diffraction. For an incident plane parallel wave $\psi_0(x, y)$ upon the specimen, the electron wave at the specimen exit face is:

$$\psi_e(x, y) = \psi_0(x, y) \cdot q(x, y)$$

where $q(x, y)$ is the 'specimen transmission function'. In the limit of a very thin sample where the amplitudes of diffracted beams are relatively weak (the kinematic approximation) and the phases of diffracted beams are modulated only weakly by the sample (weak phase object approximation), it can be shown that $q(x, y) \sim$ constant $\cdot \phi(x, y)$, where ϕ is the projected potential of the sample structure along the electron beam direction. For crystalline samples, this requires sample thicknesses less than approximately one-half the relevant axial extinction thickness (for Si at 200 kV this distance is 140 Å along $< 110 >$.) For amorphous structures of comparable atomic number, this requirement is satisfied by substantially greater thicknesses, as the variations in atomic potential with respect to the mean potential are less than in crystalline samples. The extinction distance decreases with increasing atomic number. Therefore, in order to satisfy these assumptions so that intuitive image interpretation is possible, we must analyze regions of the sample that are as thin as possible, which correspond to the regions of the cross-sectional samples that are close to the
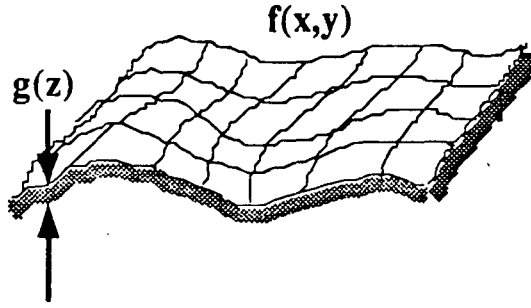
Figure 1: Interface geometry.

hole created from the ion milling process described above. We estimate that the sample thicknesses in these regions range from $\sim$ 50 to 100 Å.

Another primary consideration in HRTEM image interpretation is the effect of the microscope imaging system upon the phases and amplitudes of the diffracted beams. These effects are incorporated via an instrumental transfer function, $T(u,v)$, which is multiplied with the electron wave-function in the back focal plane of the objective lens such that

$$\tilde{\psi}_e(u,v) = \tilde{\psi}_0(u,v) * \tilde{q}(u,v) \cdot T(u,v).$$

The transfer function includes phase changes due to third-order spherical aberration (phase change proportional to the cube of spatial frequency) and objective lens defocus (phase change proportional to spatial frequency). Amplitudes are also modified due to damping envelopes arising from spatial and temporal beam incoherencies and mechanical vibrations. The form of $T(u,v)$ is thus generally very complex and HRTEM image interpretation is difficult in general requiring extensive numerical simulation of diffraction and imaging processes. However, at a specific objective lens defocus, known as Scherzer defocus, a broad band-pass of approximately constant transfer is observed at lower spatial frequencies (up to the inverse of the microscope resolution.) The magnitude of Scherzer defocus is given by $-\sqrt{1.5\lambda_e C_s}$, where λ_e is the electron wavelength and C_s is the third order spherical aberration coefficient. Thus for this defocus, the microscope imaging system is essentially neutral. (Contributions from electrons scattered by higher spatial frequencies outside of the band-pass are eliminated by insertion of an objective aperture in the back focal plane.) The magnitude of Scherzer defocus is $\sim$ -500 to -700 Å for the microscopes used here.

The final major factor to be considered here is Fresnel diffraction from the potential discontinuities at the multilayer interfaces. It can be shown by a direct optical analogue [6] that the width of the interfacial Fresnel fringe is $\sim \sqrt{\Delta f \lambda_e}$, where Δf is the magnitude of the objective lens defocus. At Scherzer defocus (and 200 kV), this fringe width is of the order 4 Å, with a likely variation due to experimental error in selecting Scherzer defocus of ± 1 Å.

Other systematic errors associated with finite sample dimensions will be discussed in the next section.

4.1.2 Interface Diffusion

We suppose that the material variations at the interface in a multilayer are described by the topography function $f(x,y)$ discussed previously, and a function $g(z)$ which describes the material variations along the $\hat{z}$-direction. These two functions are depicted in figure 1.

Analogous to the method described by Hull *et al.* [7], we measure $g(z)$ from the digitized HRTEM images by examining image intensity profiles along the $\hat{z}$-direction, as follows. Consider a rectangular region of the HRTEM image, having width L in the $\hat{x}$-direction, as shown in figure 2. [1] This particular region will have a certain number of pixels in the $\hat{x}$-direction (columns) and a certain number of pixels in the $\hat{z}$-direction (rows). We can obtain the averaged image intensity for this region by averaging the intensity profiles for each column, as shown in figure 3(a). The width w of an interface can thus be obtained by measuring the width (full-width-half-max, for example) of the

---

[1] The image quality shown in this paper is significantly degraded as compared with that of the original digitized images, due to the process used to include these images with the text.
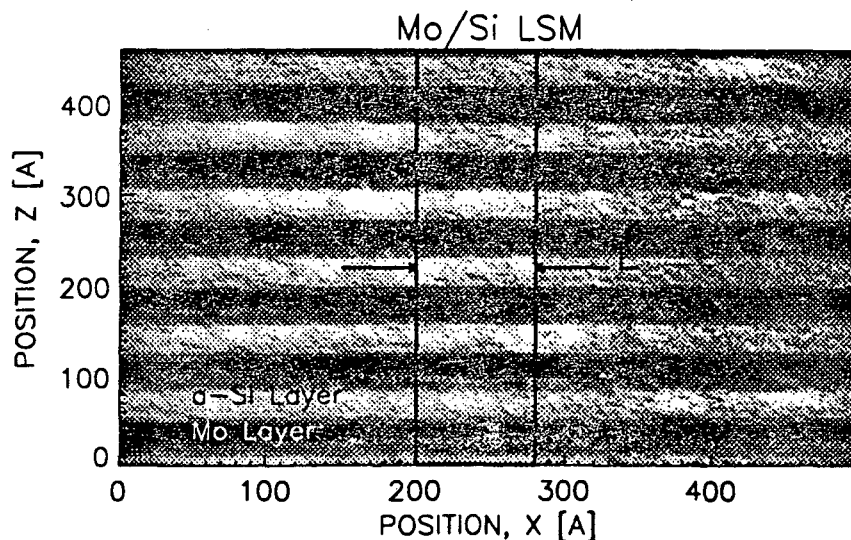
Figure 2: Digitized HRTEM image of a Mo/Si multilayer. A rectangular region of width L is highlighted.

corresponding peak in the derivative of the averaged intensity profile. The derivative of the intensity profile in figure 3(a) is shown in figure 3(b), with the interface widths indicated.

The value of w so derived will be equal to $\sigma_{diffuse}$ *plus* any contributions from interfacial roughness with spatial frequencies less than the image width L or the sample thickness t, whichever is greater. Therefore, an upper-limit on $g(z)$ is obtained in the limit $L \to 0$. However, for the case of L equal to one column width, we find that the precision with which w can be measured decreases due to noise in the images. The procedure that we follow, therefore, is to compute w as a function of L, with the L ranging from the full image width to one pixel, and then fit the $w - L$ data with a straight line to get $w(L = 0) = g(z)$. An example of this procedure is shown in figure 4, where the $w - L$ data is shown for eight interfaces of the Ru/C sample. Although there is considerable scatter in the $w - L$ data, we estimate the uncertainty in the derived interface widths to be of order $\pm .5$ Å.

Figure 5 shows the derived values of the interface widths $g(z)$ for the Ru/C sample as a function of the interface number, where interface number 0 is the Ru/C interface closest to the substrate (e.g. for this sample, with 50 bilayers, there are 100 interfaces numbered 0,1,...,99.) These data were obtained from four digitized images of the same cross-sectional sample. Evidently, the derived interface widths decrease with increasing interface number (i.e. away from the substrate.) For this particular cross-sectional sample, however, this trend is probably due not to an inherent characteristic of the multilayer, but to the fact that the cross-sectional sample thickness decreases with increasing interface number, a feature which is apparent in the original HRTEM image. (The hole resulting from the ion milling process is located furthest from the substrate.)

The decreasing sample thickness manifests itself in the derived interface widths versus interface number data shown in figure 5 because the multilayer sample may not have been perfectly aligned with respect to the incident electron beam. Orientation of the electron beam along the interfaces is achieved by aligning the silicon substrate, but the multilayer orientation is not necessarily the same in the thinned TEM sample. This will result in an apparent interface width $t\theta'$, where θ' is the misorientation angle. With a maximum likely misorientation of say $\theta' = 3°$ and $t = 100$ Å, the resulting maximum systematic error in the defined interface width would be of order 3 Å.

The effect of sample thickness on derived interface width was also seen in a second image of another TEM sample of the same Ru/C multilayer. For this second image, however, the 'ion-milling-hole' was located approximately midway from the substrate to the surface of the multilayer, which enabled interface widths to be derived for almost all of the 100 interfaces. The derived interface widths from this sample show a minimum near the center of the sample, corresponding to the location of the ion-milling-hole and thus the thinnest region of the sample.

AVERAGED INTERFACE PROFILE

Averaged over 80.0 A starting at (200.0,0.0) A.

DERIVATIVE OF AVERAGED INTERFACE PROFILE

Averaged over 80.0 A starting at (200.0,0.0) A.
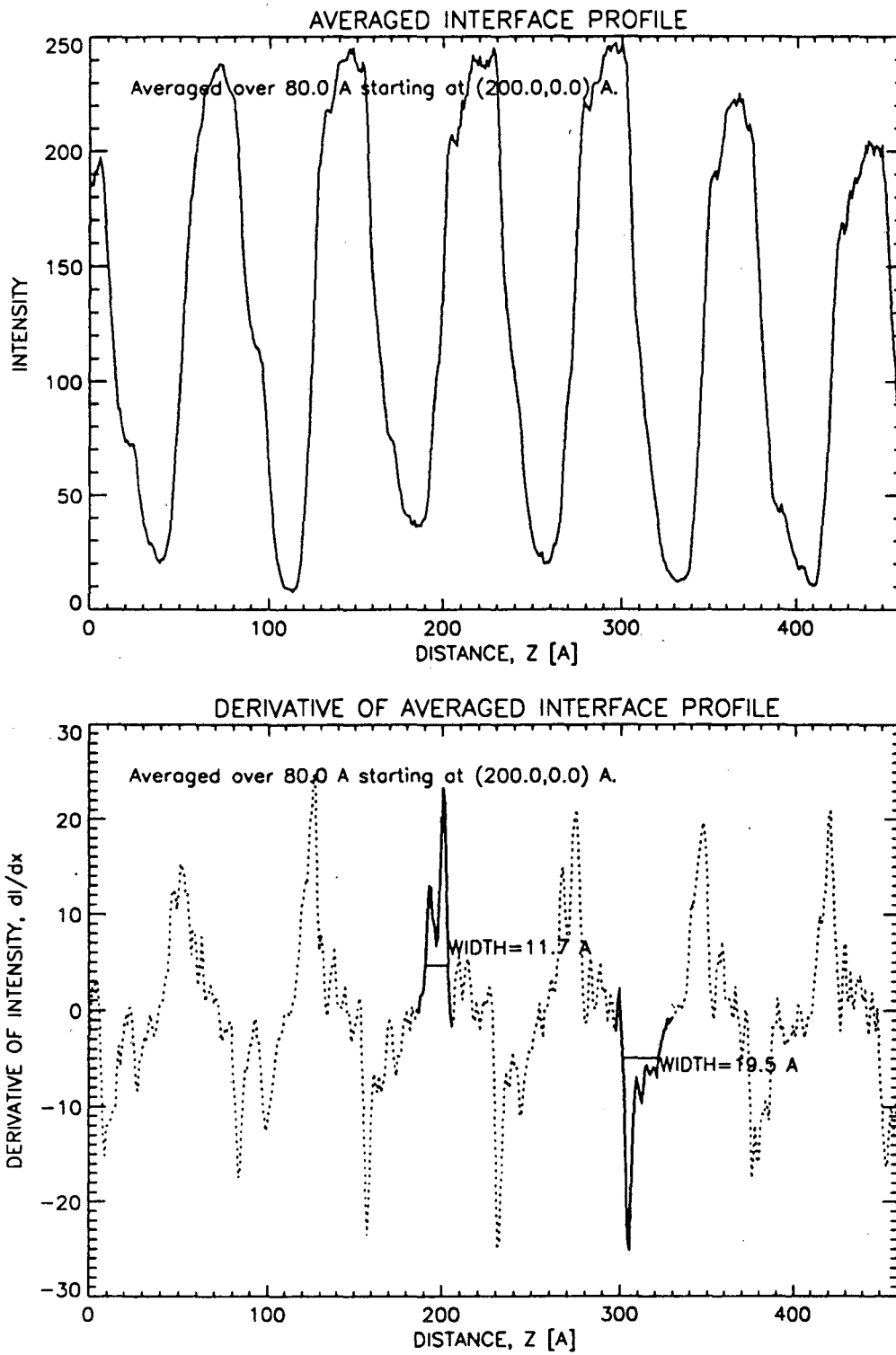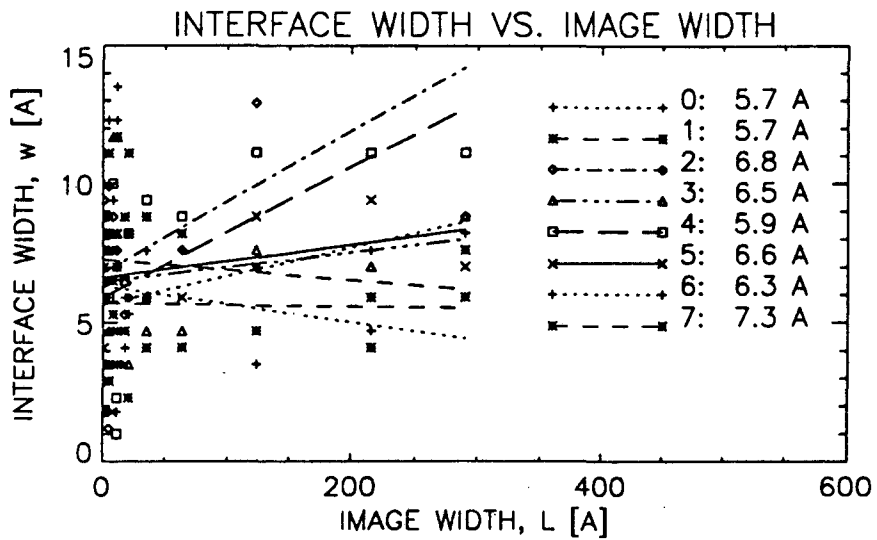
WIDTH=11.7 A

WIDTH=19.5 A

Figure 3: (a) Averaged intensity profile from the image shown in figure 2. (b) Derivative of averaged interface profile. Interface widths, defined for this particular case as the full-width at quarter-maximum, are indicated.

INTERFACE WIDTH VS. IMAGE WIDTH

0:	5.7 A
1:	5.7 A
2:	6.8 A
3:	6.5 A
4:	5.9 A
5:	6.6 A
6:	6.3 A
7:	7.3 A

IMAGE WIDTH, L [A]

Sample: Ru/C. Image #1.

Figure 4: Interface width (w) versus image width (L), for eight interfaces from an HRTEM image of the Ru/C sample. The straight lines are least-squares fits to the data. The legend identifies the interface number and derived values of $w(L = 0)$.

DERIVED INTERFACE WIDTHS

Ru/C ; <g(z)>=4.6 A
C/Ru ; <g(z)>=4.5 A
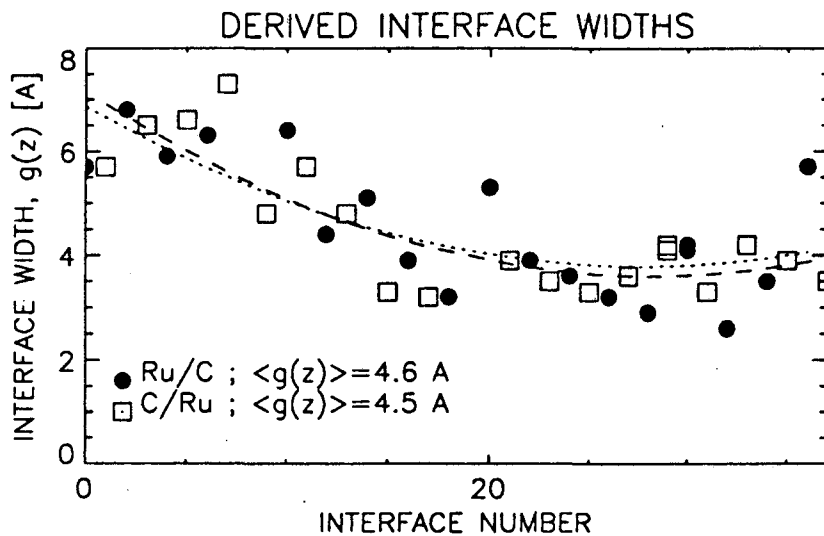
INTERFACE NUMBER

Sample: Ru/C. Images #1-4.

Figure 5: Interface width $g(z)$ versus interface number for the Ru/C sample. The lines are least-squares polynomial fits to the data.

4.1.3 Interface Topography

We now wish to measure the interface topography function $f(x,y)$. From the projected HRTEM images, however, we can of course measure only a one-dimensional function $f'(x)$, which is equal to $f(x,y)$ averaged over the sample thickness t in the $\hat{y}$-direction. Nonetheless, we assume for the time being that for small thicknesses (i.e. $t \sim 50\text{-}100$ Å), the function $f'(x)$ approximates the true profile $f(x)$. We further assume that the topography function is isotropic such that $f(x,y) = f(x)$.

We measure the topography from the digitized images using a contour algorithm, whereby (suitably chosen) iso-intensity contours represent the topography function $f(x)$. Figure 6(a) shows an HRTEM image for a Mo/Si sample and figure 6(b) shows the derived iso-intensity contours. Due to the fact that the contour algorithm results in non-equally-spaced (along $\hat{x}$) interface height profiles, the profiles were fit (using cubic-spline interpolation) with 1024 equal-spaced points for analysis.

The one-dimensional power-spectral-density (PSD) function $S(f_x)$ is computed from $f(x)$ using a fast Fourier transform (FFT) algorithm. Since the 1024-element profile contains spatial frequencies smaller than the resolution limit of the microscope, the PSD was computed only for spatial frequencies larger than this resolution limit. Shown in figure 7 is the interface topography function $f(x)$ and the corresponding PSD, for one interface of the Mo/Si sample shown in figure 6.

The value of σ_{rough} is then computed from $S(f_x)$ through

$$\sigma^2 = \int_{f_{\min}}^{f_{\max}} S(f_x) df_x. \tag{6}$$

The σ_{rough} values so derived are shown in figure 8 for the Ru/C sample.

A recent paper by Church [8] discusses the power spectra of rough surfaces in terms of a fractal power-spectral-density function, of the form

$$S(f_x) = K_n / f_x^n \text{ with } 1 < n < 3. \tag{7}$$

The motivation is that highly polished optical surfaces should show fractal characteristics over a limited range of spatial frequencies. Indeed, we have fit the power spectra of the multilayer interfaces derived from HRTEM images, using a least-squares curve-fitting algorithm, with the fractal form form given by equation 7. An example of such a fit is shown as the dotted line in figure 7(b). The derived fractal fit parameters K_n and n are shown versus interface number in figure 9 for the Ru/C sample.

From equation 7, the two-dimensional PSD can be calculated (assuming that the topography is isotropic) from [8]

$$S(\mathbf{f}) = \frac{\Gamma[(n+1)/2]}{2\Gamma(1/2)\Gamma(n/2)} \cdot \frac{K_n}{f_x^{n+1}} \tag{8}$$

It is this equation that would be inserted into equation 5 in order to calculate the non-specular scattered power distribution.

Also, from the fractal fit to the measured PSD it is possible to extrapolate to a particular range of spatial wavelengths (assuming that the topography warrants such an extrapolation) in order to compute the spatial-frequency-dependent value of σ_{rough} (using equation 6):

$$\sigma_{\text{rough}}(L_{\min}, L_{\max}) = \sqrt{\frac{K_n}{n-1}} \left(L_{\max}^{n-1} - L_{\min}^{n-1} \right)^{1/2}, \tag{9}$$

where $L_{\min}$ and $L_{\max}$ are the minimum and maximum spatial wavelengths under consideration. This idea will be described further in the next section.

4.2 Optical Properties

We now wish to relate the measured structural properties (σ_{diffuse}, σ_{rough}, and $S(f_x)$) to the measured optical properties, namely the specular reflectance and the non-specular scattering. We must first consider, however, that these optical properties will be sensitive to a finite range of spatial frequencies, which demands that the value of σ_{rough} should be determined for the appropriate spatial frequency range.

CONTOUR LEVEL: 145
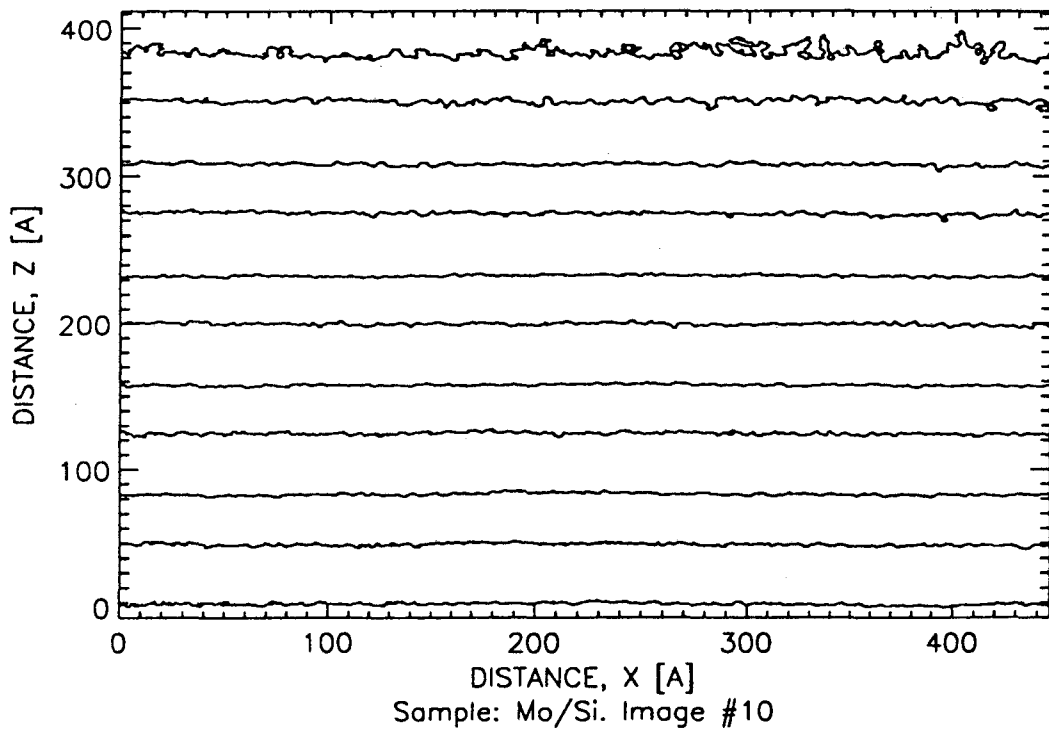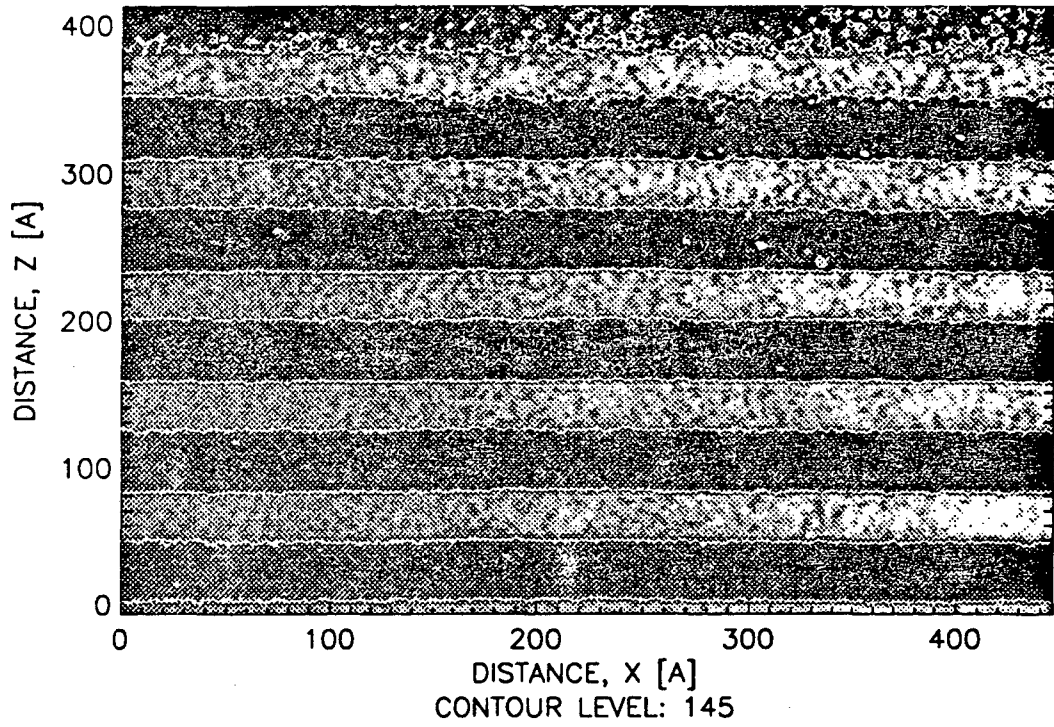
Sample: Mo/Si. Image #10

Figure 6: (a) Digitized HRTEM image of a Mo/Si sample with iso-intensity contours superimposed. (b) Iso-intensity contours, which represent the interface topography function $f(x)$.

PROFILE

$\sigma = 1.24$ A

HEIGHT, z [A]

SCAN LENGTH, x [A]

Sample: Mo/Si. Interface #5.

POWER-SPECTRAL-DENSITY

$\sigma=0.8574$ A, $\ell=35.2957$ A

$S(f) = K_n/f^n$

$K_n=0.0272$, n=1.3046

POWER-SPECTRAL-DENSITY, S(f) [A^3]

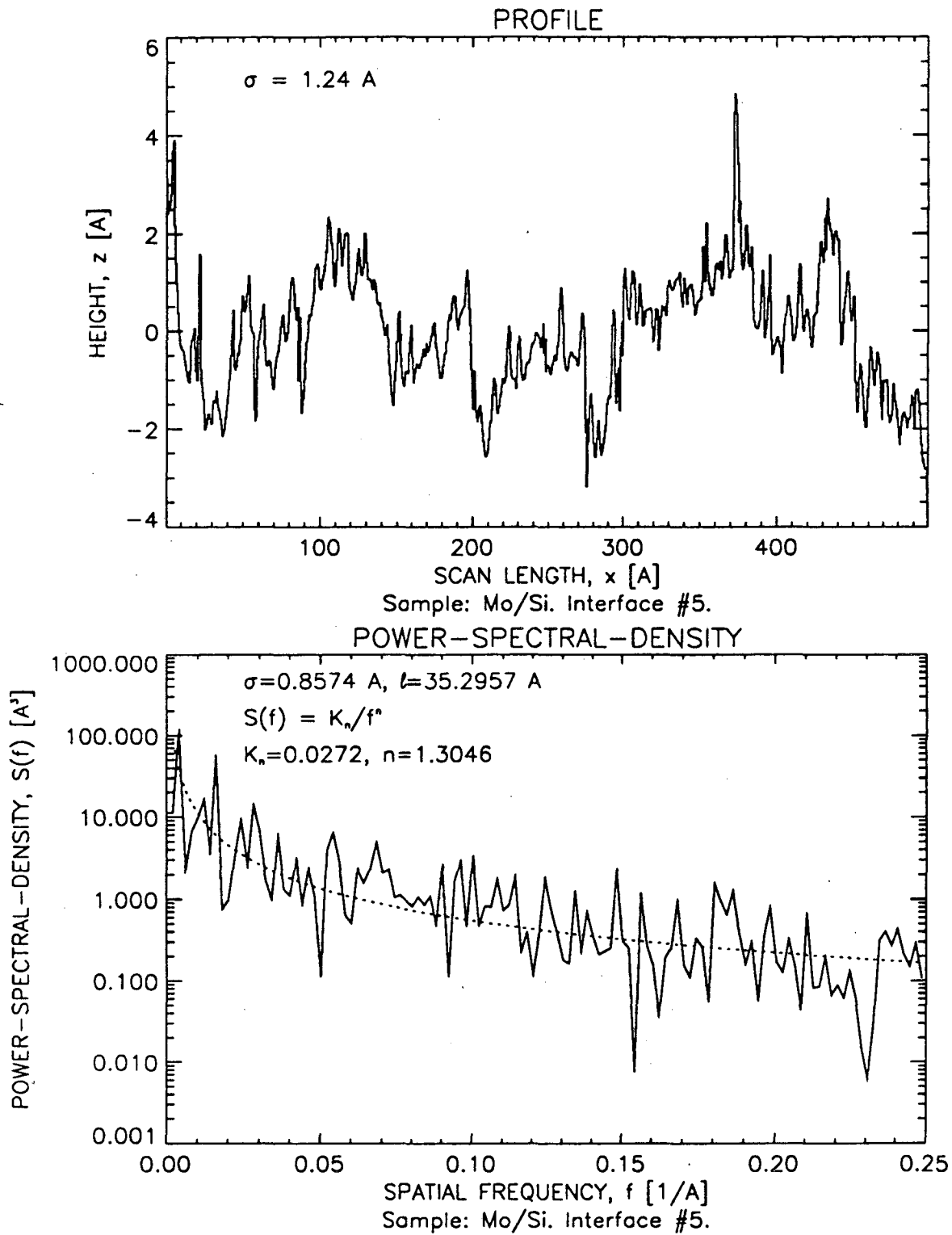SPATIAL FREQUENCY, f [1/A]

Sample: Mo/Si. Interface #5.

Figure 7: (a) Interface topography function $f(x)$ and (b) power-spectral-density, for one interface of the Mo/Si sample shown in figure 7. The dotted line in (b) is a least-squares fractal fit to the PSD.
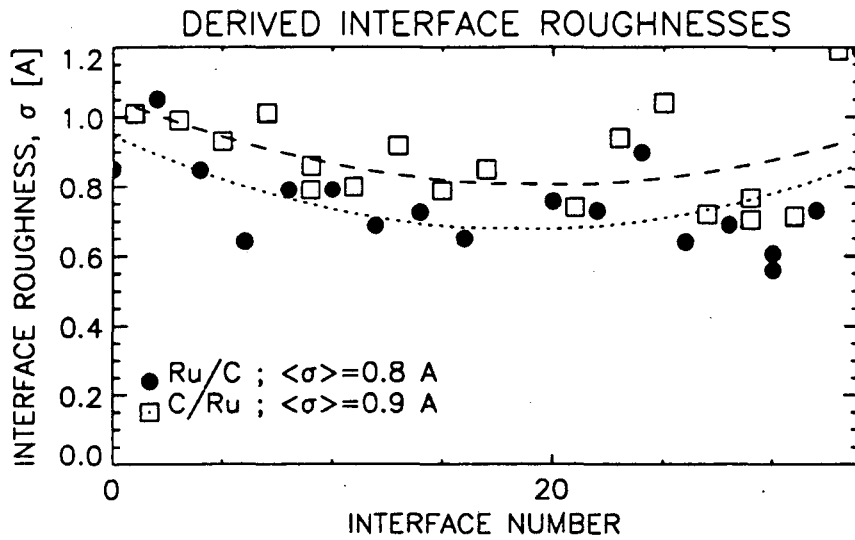
DERIVED INTERFACE ROUGHNESSES

Sample: Ru/C. Images #1−4.

Figure 8: Derived values of σ_{rough} for the Ru/C sample. The σ_{rough} values for the Ru-on-C and C-on-Ru interfaces are shown separately.

The relationship between spatial frequencies at the interface (or surface) and the direction of scattered light may be determined in a simple way using the grating equation. That is, from the grating equation we may relate the geometry of the optical measurement (i.e., the incidence angle, wavelength, and detector solid angle) to spatial frequencies at the interface. Specifically, for the case of a specular reflectance versus incidence angle measurement, the value of σ_{rough} which would be used in equations 2 and 3, would depend not only on the detector collection angle and the wavelength of light being used, but would also vary with incidence angle. For example, figure 10 shows the range of spatial wavelengths to which a specular reflectance measurement is sensitive, as a function of wavelength from $\lambda = 1.54$ Å (Cu-Kα) to 200 Å, for incidence angles in the range of 0° (normal incidence) to θ_{max}, with θ_{max} ranging from 60° to 90°, and for a detector collection angle of .2° (specularly reflected light is thus defined to be those rays for which $|\theta'| \leq .1°$, where θ' is the scattering angle with respect to the specular direction $-\theta_0$.) We see from the figure that at a given photon wavelength, the range of spatial wavelengths increases with increasing θ_{max}. Also, for a constant θ_{max} the maximum spatial wavelength increases by a large amount as the photon wavelength increases from 1.54 Å to 200 Å. When computing the integral in equation 6, however, we must also consider that the σ values determined from reflectance data are obtained by examining the reflectance in the vicinity of the Bragg peaks; these peaks are measured near normal incidence at XUV wavelengths, but at grazing incidence for Cu-Kα. Consequently, the value of θ_{max} is considerably larger for Cu-Kα than for XUV wavelengths, so the variation in the range of spatial wavelengths – and the difference in σ_{rough} values computed from equation 6 – will be somewhat reduced. In particular, for the x-ray and XUV measurements in this work (which have different detector collection angles,) the spatial wavelengths to which the reflectance is sensitive range from ∼1.54 Å – 2.5 μm for λ=1.54 Å, and from ∼135 Å – 10.0 μm for λ=135 Å.

As mentioned in the last section, the fractal PSD function provides an analytic method (equation 9) for calculating the σ_{rough} value appropriate for a given specular reflectance measurement (i.e. a given range of spatial wavelengths.) Shown in figure 11 are the calculated σ_{rough} values versus incidence angle for λ=1.54 Å and 135.0 Å, using the fractal fit parameters derived for one of the Mo/Si multilayer samples, and using the spatial wavelength ranges mentioned above. Note first that the σ_{rough} values for 135 Å are ∼50% larger than the values for 1.54 Å over most of the range of θ. This difference in σ_{rough} with wavelength will vary considerably with the fractal power n. Second, the σ_{rough} values are approximately constant over most of the range of incidence angles but increase sharply in the region of grazing incidence. Therefore, the comparison between the measured reflectance and the reflectance calculated using equations 2 and 3 should reveal that for long wavelength measurements near normal incidence, a constant value of σ_{rough} (as a function of incidence angle) does not give significantly different results compared with σ_{rough} depending
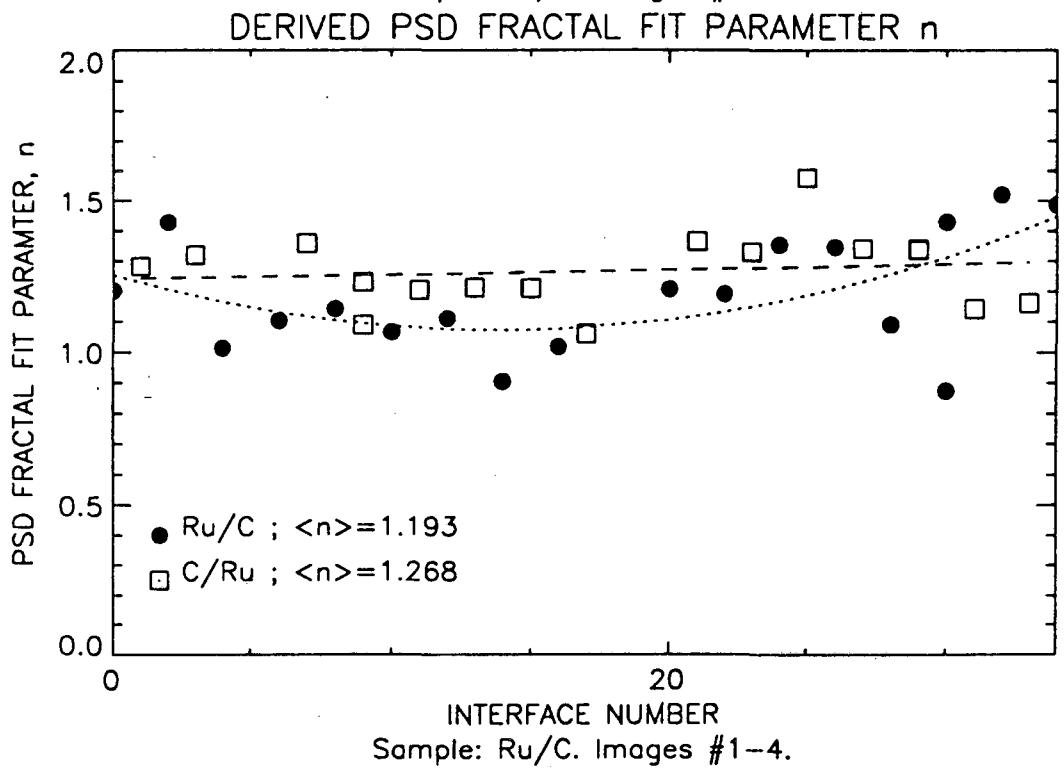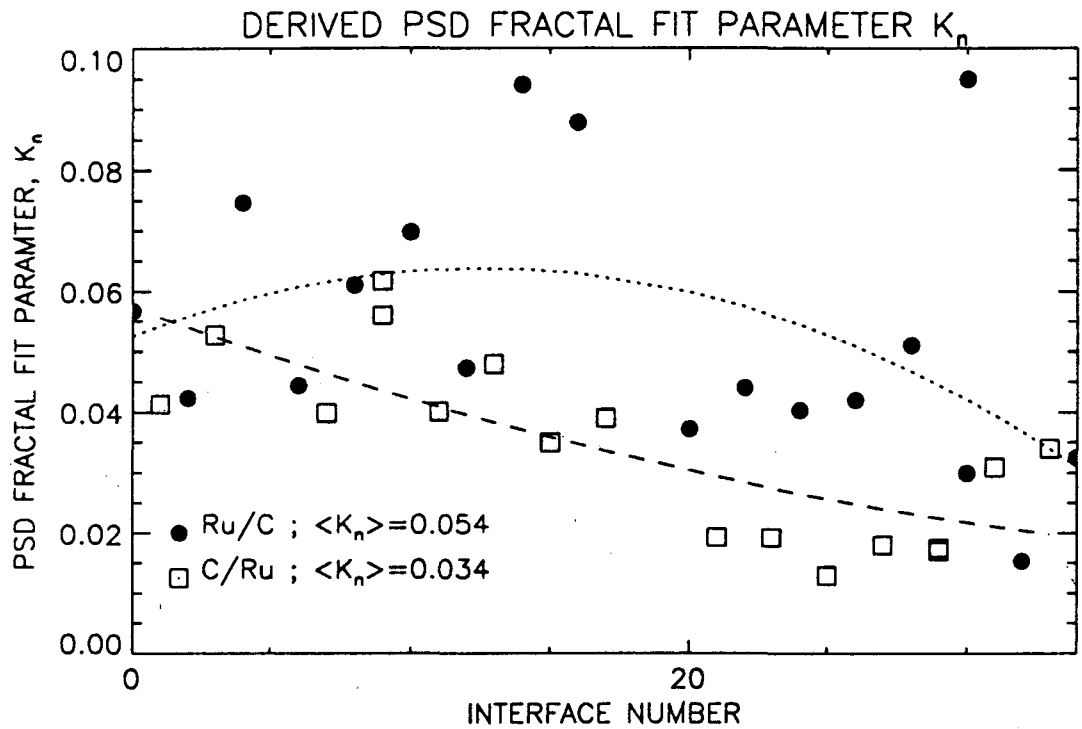
Figure 9: Derived fractal fit parameters (a) K_n and (b) n for the Ru/C sample. The derived parameters for the Ru-on-C and C-on-Ru interfaces are shown separately.

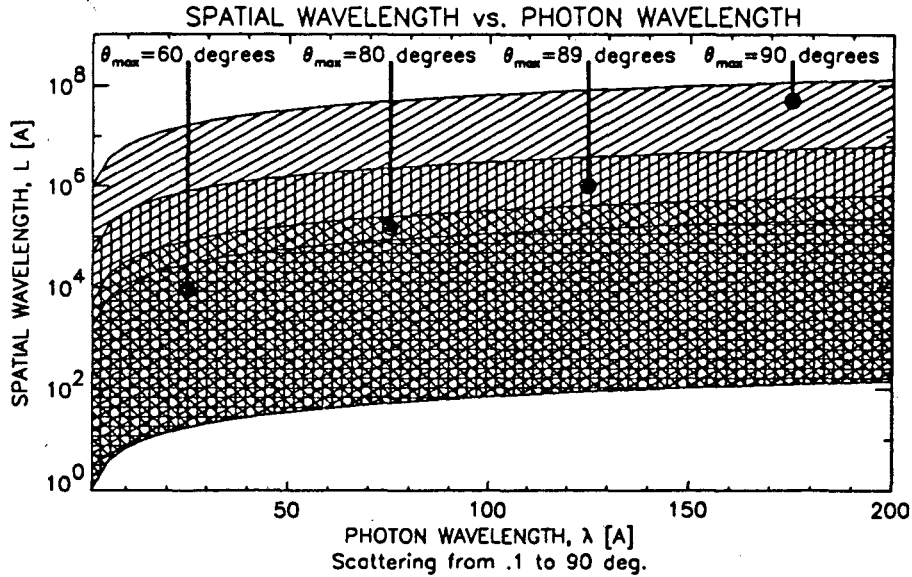**SPATIAL WAVELENGTH vs. PHOTON WAVELENGTH**

Figure 10: Spatial wavelength range to which specular reflectance measurements are sensitive as a function of wavelength, assuming a detector collection angle of .2°.

on incidence angle, whereas for Cu-Kα reflectance measurements (at grazing incidence, θ=80-90°) these comparisons should reveal that a σ_{rough} which increases with incidence angle is required.

Indeed, we find this last result to be the case. For example, shown in figure 12 are the measured XUV and x-ray reflectance versus incidence angle curves for the Ru/C sample, along with the fits to these curves. For each wavelength, fits were obtained using the optical constants from Henke *et al.* [9] (for this sample) and the instrumental resolutions were included in the calculations [10]. In this case, we find good agreement using constant σ values of 7 Å for the XUV measurements (λ=44.7 - 82.1 Å), but for the Cu-K measurements, we get the best agreement using $\sigma = \sigma_{rough}(\theta)$+1.5 Å, where $\sigma_{rough}(\theta)$ is given by equation 9 with L_{min} and L_{max} determined from the measurement geometry. The agreement at λ=1.54 Å is not perfect, however. Interface profile functions $p(z)$ other than an error function could improve the agreement without significantly degrading the agreement at XUV wavelengths, as the longer wavelength measurements are not particularly sensitive to the exact form of $p(z)$. The results for the other samples are summarized in the next section.

5   RESULTS

We have analyzed HRTEM images for each of the three samples described in section 3. For each sample, several images were examined, and values for $g(z)$ and σ_{rough} versus interface number were obtained. Additionally, the power spectra for each interface were computed and fractal fits were obtained.

We find that in the case of the Mo/Si samples, the $\sigma_{diffuse}$ values are significantly different for the Mo-on-Si interfaces and the Si-on-Mo interfaces. This result and the values for $< g(z) >$ we derive (table 1) are consistent with previously reported results [11]. For the Ru/C sample, we find no such asymmetry, also consistent with previous results for this system [12]. We also find no correlation between any of the structural parameters and interface number, for all three samples. (Such a correlation might arise from interface smoothing as more layers are added during deposition, for example.) We have therefore computed the *average* values of $g(z)$, K_n and n, for each sample, and for each type of interface (e.g. Mo/Si, Si/Mo, Ru/C, C/Ru.) These results are summarized in table 1.

From $< g(z) >$, $\sigma_{diffuse}$ was computed assuming that the derivative of the interface profile is a Gaussian, such that $\sigma_{diffuse}=< g(z) > / \left(2\sqrt{2\ln(M)}\right)$, where M=0.5 or 0.25, for $< g(z) >$ corresponding to the full-width at half-max or quarter-max, respectively. From the fractal fit parameters $< K_n >$ and $< n >$, σ_{rough} values were computed from equation 9, using the range of spatial wavelengths appropriate for the Cu-Kα and the XUV reflectance measurements,
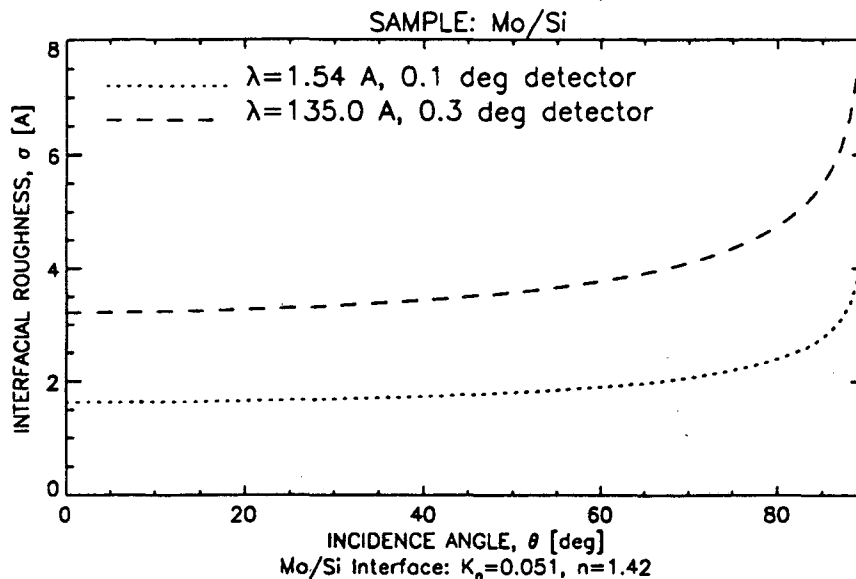
Figure 11: Calculated σ_{rough} as a function of incidence angle, using the fractal fit parameters derived from a Mo/Si multilayer sample. The detector collection angles indicated at each wavelength correspond to the actual values for the x-ray and XUV reflectance measurements reported here.

respectively. (The average σ_{rough} values for the three samples as computed for the actual range of spatial wavelengths associated with HRTEM were 0.8, 1.0, and 1.3 Å.) Finally, σ_{total} was computed from equation 3. These results are shown in table 1 as well. The uncertainties in these σ values associated with the data reduction techniques we estimate to be of the order ±1 Å. On the other hand, the systematic errors associated with the image interpretation itself we expect to be larger, of order ~ ±4 Å for the interface widths, and a comparable number for the interface roughness values due to averaging the topography over the sample thickness.

Also shown in table 1 are the average σ values derived from XUV and Cu-Kα reflectance measurements. These values were obtained using a model based on the recursive technique, with equation 1 describing the reflectance loss due to interface imperfections and assuming an error function interface profile. (Asymmetric interface widths, as were measured from the HRTEM images for the Mo/Si samples, don't significantly affect the fits for XUV wavelengths.) The model has several adjustable parameters in addition to σ, including the optical constants and layer thicknesses. At $\lambda=1.54$ Å, the optical data from Henke et al. [9] were used, and the layer thicknesses were determined with very high precision. These thicknesses were then used in the fits at long wavelengths, where the thicknesses, optical constants, and σ values are strongly coupled. The optical constants used at long wavelengths were those from [9] for the Ru/C sample, and from [13] for Mo/Si. Although the derived σ values will depend on the optical constants used, the optical constants can be checked for accuracy by demanding that the theoretical reflectance curves agree with measurement near grazing incidence, not merely in the vicinity of the Bragg peaks. [2] The uncertainty in the σ values derived from the reflectance data is ~ ±.25 Å, though there may be larger systematic errors, due to systematic measurement errors or inaccurate optical constants.

In light of all the possible systematic errors mentioned above, the σ values deduced from reflectance measurements are reasonably close to those derived from the HRTEM analysis, though the discrepancy is larger than the nominal experimental uncertainties just described. Also, the variation between the σ values derived from reflectance measurements at x-ray and XUV wavelengths is considerably larger than the analogous variation in the σ values derived from HRTEM. Furthermore, the large difference in $\sigma_{diffuse}$ between the Ru/C sample and the Mo/Si samples is not at all evident in the reflectance data. These discrepancies can be due to errors in deriving σ values from reflectance data, to deficiencies in the model relating the structural and optical properties, or to systematic errors associated with the HRTEM image analysis.

---

[2] For the Ru/C sample, it was necessary to use layer thicknesses that differed by 0.9 Å from the values determined from Cu-Kα measurements. This suggests that the densities assumed (which correspond to the bulk material values) in the conversion from the Henke atomic scattering factors to optical constants are incorrect for one or both of these materials.
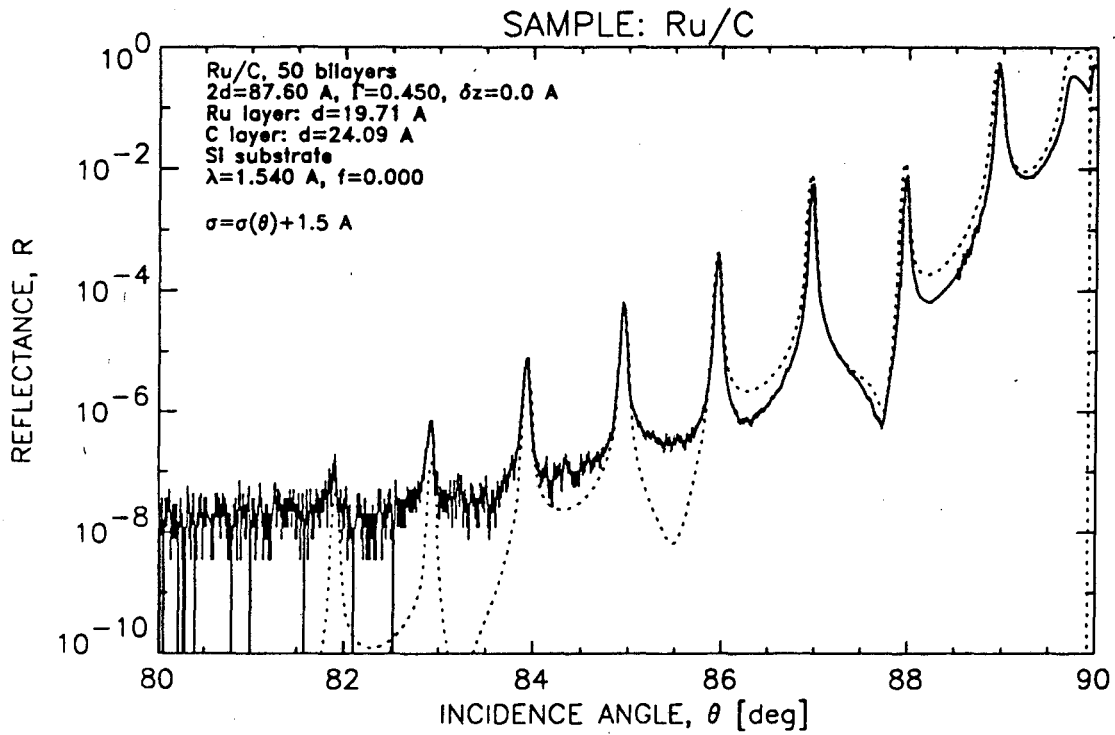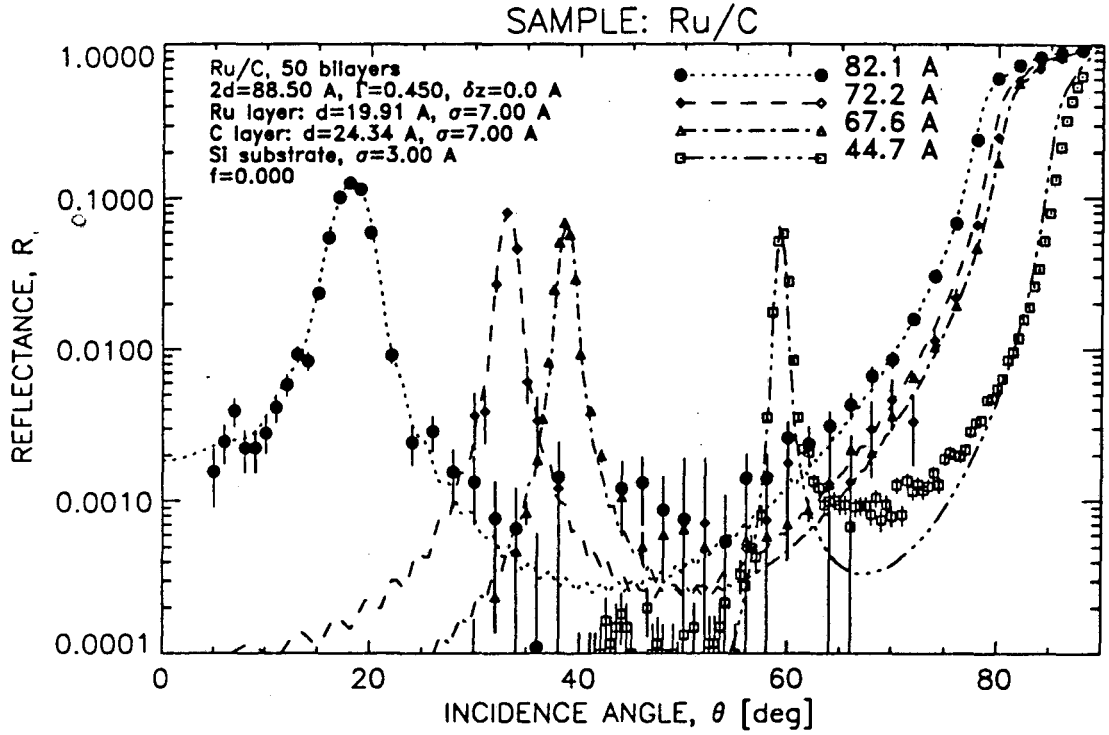
Figure 12: (a) XUV and (b) Cu-K reflectance versus incidence angle data for the Ru/C sample, and the associated fits.

Sample, Interface	HRTEM									Reflectance	
	$<K_n>$	$<n>$	σ_{rough}		$<g(z)>$	σ_{diff}	σ_{total}		$<\sigma>$		
			Cu-Kα	XUV			Cu-Kα	XUV	Cu-Kα	XUV	
Ru/C (Ru/C)	.043	1.28	1.6 Å	1.7 Å	3.9 Å	1.7 Å	3.3 Å	3.4 Å		
(C/Ru)	.021	1.32	1.3 Å	1.4 Å	3.8 Å	1.6 Å	2.9 Å	3.0 Å		
Average			1.4 Å	1.5 Å		1.6 Å	3.1 Å	3.2 Å	2.5 Å	7 Å
Mo/Si (Mo/Si)	.047	1.38	2.4 Å	3.0 Å	19.7 Å	8.4 Å	10.8 Å	11.4 Å		
(Si/Mo)	.014	1.35	1.2 Å	1.4 Å	9.0 Å	3.8 Å	5.0 Å	5.2 Å		
Average			1.8 Å	2.2 Å		6.1 Å	7.9 Å	8.3 Å	3 Å	10 Å
Mo/Si (Mo/Si)	.051	1.42	2.9 Å	3.8 Å	19.1 Å	5.7 Å	8.6 Å	9.5 Å		
(Si/Mo)	.067	1.31	2.2 Å	2.6 Å	16.3 Å	4.9 Å	7.1 Å	7.5 Å		
Average			2.5 Å	3.2 Å		5.3 Å	7.8 Å	8.5 Å	2 Å	7 Å

Table 1: Summary of results. The structural parameters derived from HRTEM image analysis are compared with those derived from reflectance measurements. The σ_{rough} values (and hence the σ_{total} values) were computed from the PSD fit parameters K_n and n using equation 9, for the spatial wavelength ranges appropriate to reflectance measurements made using Cu-Kα and XUV radiation, as indicated in the text.

As mentioned above, the parameters in the model for reflectance can be strongly coupled, so small inaccuracies in layer thicknesses or optical constants, or systematic measurement errors [10] can result in significant inaccuracies in derived σ values. The possibility of errors in the XUV and x-ray derived σ values can therefore not be ruled out.

Deficiencies in the model may be related to the form of the assumed interface profile function $p(z)$, as mentioned previously; we are presently investigating alternative interface profile functions. We have also examined graded interfaces (e.g. many thin layers at each interface, with each *interlayer* having different optical constants) using from one to ten interlayers, but we find that the agreement is not significantly improved. In fact the shape of the resulting reflectance curve at 1.54 Å is quite different from that which is measured. The assumption that the bilayers near the substrate are identical (optically) to those near the surface may explain some of discrepancy, or it may simply be the case that the first order scattering theory outlined in section 1 is inadequate.

, The systematic errors associated with HRTEM image interpretation have been described above. In general, we expect that these errors would result in (i) $\sigma_{diffuse}$ values that are too high, due mainly to Fresnel fringe effects, sample misorientation, and the inclusion of roughness with spatial wavelengths less than the sample thickness, and (ii) σ_{rough} values that are too low due to averaging the topography over the sample thickness. Averaging the topography over the sample thickness will result in an inaccurate power-spectral-density, in general, and will tend to reduce the derived σ_{rough} values, as the resulting fractal parameter n will be too small. The contrast between the x-ray and XUV σ_{rough} values increases with increasing n. Although the extrapolation of the PSD deduced from HRTEM to larger spatial wavelengths (i.e. $\sim$10 μm) may by unwarranted, a larger n value coupled with smaller $\sigma_{diffuse}$ values would result in σ_{total} values that are more consistent with those determined from reflectance measurements.

6   CONCLUSION

We have shown how structural properties associated with the interface imperfections in XUV multilayer reflectors can be deduced from HRTEM images, using a variety of analysis techniques. We have compared these structural parameters with those derived from comparisons of XUV and x-ray specular reflectance measurements with calculations using a first-order vector scattering theory, and find that the two sets of parameters agree, in light of the estimated magnitude of systematic errors associated with the measurement and interpretation techniques. By extrapolating the power-spectral-density function measured from HRTEM images to the spatial wavelength ranges appropriate to reflectance measurements, we find, however, that the contrast between the inferred x-ray and XUV interface widths is not in agreement with the measured values. Furthermore, the large difference in diffusion widths between the Ru/C sample and the Mo/Si samples is not at all evident in the reflectance data.

We are continuing this investigation in order to resolve these discrepancies. We are proceeding with further HRTEM analysis, and intend to more precisely estimate the magnitude of all systematic errors associated with image interpretation. Measurements of the *surface* topography of these multilayers, using a scanning, tunneling electron microscope and perhaps optical techniques (as has been investigated by Spiller *et al.* [14]), may afford a more accurate measure of the topography function over the range of spatial frequencies relevant to XUV reflectance, however it is not clear that the surface and interface topographies are identical. We are also planning non-specular scattering measurements to be performed using synchrotron radiation, which will also be used to estimate the interface PSD function. Finally, further refinements in the reflectance calculation techniques, the reflectance measurements, and more accurate optical constants will also help to elucidate the source of the discrepancy.

7   ACKNOWLEDGEMENTS

References

[1] D. L. Windt and J. B. Kortright, 'XUV optical characterization of thin film and multilayer reflectors' *SPIE*, **1160**, 246 (1989)

[2] J. M. Bennett and L. Mattsson, 'Introduction to surface roughness and scattering',Optical Society of America, Washington, D.C., 1989

[3] D. G. Stearns, 'The scattering of x-rays from nonideal multilayer structures', *J. Appl. Phys.*, **65**, 491 (1988)

[4] M. Born and E. Wolf, *Principles of Optics*, Sixth Edition, Pergamon Press, 1980.

[5] D. L. Windt and R. C. Catura, 'Multilayer characterization at LPARL', *Proc. SPIE*, **984**, 82 (1988)

[6] D. R. Clarke, 'On the detection of thin intergranular films by electron microscopy', *Ultramicroscopy*, **4**, 33 (1979)

[7] R. Hull, K. W. Carey, and G. A. Reid, 'Theoretical and experimental description of interface structure', *Mat. Res. Soc. Symp. Proc.*, **77**, 455 (1987)

[8] E. L. Church, 'Fractal surface finish', *App. Opt.*, **27**, 1518 (1988)

[9] B. L. Henke, J. C. Davis, E. M. Gullikson, and R. C. C. Perera, *A preliminary report on x-ray photoabsorption coefficients and atomic scattering factors for 92 elements in the 10-10,000 eV region*, LBL-26259, UC-411, November 1988

[10] D. L. Windt, W. K. Waskiewicz, G. D. Kubiak, T. W. Barbee, Jr., and R. Watts, 'XUV characterization comparison of Mo/Si multilayer coatings', these Proceedings.

[11] D. G. Stearns, M. B. Stearns, Y. Cheng, J. H. Smith, and N. M. Ceglio, 'Thermally induced structural modification of Mo-Si multilayers', *J. Appl. Phys.*, **67**, 2415 (1990)

[12] T. D. Nguyen, R. Gronsky, and J. B. Kortright, 'Microstructure and stability comparison of nanometer period W/C, WC/C, and Ru/C multilayer structures', to appear in *Mat. Res. Soc. Symp. Proc.*, **187**, (1990)

[13] D. L. Windt, 'XUV optical constants of single-crystal GaAs and sputtered C, Si, Cr_3C_2, Mo, and W', accepted for publication in *App. Opt.* (1990)

[14] E. Spiller, R. McCorkle, J. Wilczynski, L. Golub, G. Nystrom, P. Takacz, and C. Welch, 'Imaging performance and tests of soft x-ray telescopes', these Proceedings.

LAWRENCE BERKELEY LABORATORY
UNIVERSITY OF CALIFORNIA
INFORMATION RESOURCES DEPARTMENT
1 CYCLOTRON ROAD
BERKELEY, CALIFORNIA 94720